J. Fluid Mech. (2001), *vol.* 427, *pp.* 275–297. Printed in the United Kingdom

Transient response of a compressible fluid in a rapidly rotating circular pipe

By JUN SANG PARK[1] AND JAE MIN HYUN[2]†

[1] Department of Mechanical Engineering, Halla Institute of Technology, San 66, HeungUp, Wonju, Kangwondo 220-712, South Korea

[2] Department of Mechanical Engineering, Korea Advanced Institute of Science & Technology, 373-1 Kusong-Dong, Yusung-gu, Taejon 305-701, South Korea

(Received 1 April 1999 and in revised form 10 August 2000)

The transient adjustment process of a compressible fluid in a rapidly rotating pipe is studied. The system Ekman number E is small, and the assumptions of small Mach number and the heavy-gas limit ($\gamma = 1.0$) are invoked. Fluid motion is generated by imposing a step-change perturbation in the temperature at the pipe wall T_w. Comprehensive analytical solutions are obtained by deploying the matched asymptotic technique with proper timescales $O(E^{-1/2})$ and $O(E^{-1})$. These analytical solutions are shown to be consistent with corresponding full numerical solutions. The detailed profiles of major variables are delineated, and evolution of velocity and temperature fields is portrayed. At moderate times, the entire flow field can be divided into two regions. In the inner inviscid region, thermo-acoustic compression takes place, and the process is isothermal–isentropic with the angular momentum being conserved. In the outer viscous region, diffusion of angular momentum occurs. The principal dynamic mechanisms are discussed, and physical rationalizations are offered. The essential differences between the responses of a compressible and an incompressible fluid are highlighted.

The issue of stability of the analytically obtained flow is addressed by undertaking a formal stability analysis. It is illustrated that, within the range of parameters of present concern, the flow is stable when $\varepsilon \sim O(E)$.

1. Introduction

This paper is concerned with the flow of a viscous, thermally conducting compressible gas contained in a rapidly rotating infinitely long cylindrical pipe. In the basic state, the pipe rotates steadily about the longitudinal central axis at constant rotation rate, and the pipe and gas are in thermal equilibrium at constant temperature T_{00}^{*}. Here, the rotation rate is sufficiently high that the compressibility effect, as represented by finite values of the Mach number M of the fluid system, is significant. This also implies that the effective acceleration in the radial direction overwhelms the conventional Earth's gravitational acceleration. Under these circumstances, the gas in the pipe is in rigid-body rotation, and the density increases exponentially in the radially outward direction (e.g. Sakurai & Matsuda 1974; Bark & Bark 1976; Miles 1981). Interest is focused on the flow which arises out of this basic state of rigid-body rotation when a small temperature perturbation is imposed on the pipe wall.

† To whom correspondence should be addressed: e-mail jmhyun@cais.kaist.ac.kr

The basic physics of the problem setting is relevant to high-speed rotating machinery (e.g. Torii & Yang 1994) and classical geophysical and astrophysical fluid systems (e.g. Gans 1975). Several studies have been reported on compressible flows from an initial state of solid-body rotation. Most were concerned with wave motions of an inviscid, perfect gas (e.g. Frankel 1959; Morton & Shaughnessy 1972; Gans 1974; Miles 1981). The stability of compressible swirling flows was dealt with by Gans (1975) and Lalas (1975). It is important to note that these previous investigations used inviscid approaches; therefore, little serious attempt was made to illuminate the viscous–inviscid interaction over the diffusive timescale. It is stressed that the thrust of this paper is to explore the transient diffusive flow process from one established basic state to another.

It should be emphasized from the outset that, if the fluid is incompressible, the formulation is readily reduced to that of a straightforward axisymmetric diffusion problem. In this case, the transient flow can be described by using the Fourier–Bessel series solution (e.g. Batchelor 1967), which is characterized by the diffusion timescale, as can easily be inferred from the nature of the physical process.

For a compressible fluid, however, the whole picture is substantially different from the above-described simplistic diffusion process of an incompressible fluid. Of major importance now is the strong dynamic interplay between azimuthal and meridional velocities and thermal fields. In this paper, analytical methods are utilized to study time-dependent flows of a compressible fluid when the external perturbation is small so that linearization is permitted. Because of the high rotation rate of the pipe, the overall system Ekman number is very small. The results of the analysis clearly illustrate that, at early times after a small perturbation is given to the pipe wall, the flow field can be divided into two distinctive zones: a diffusive boundary layer near the pipe wall and an inner inviscid core. This early-time behaviour is a peculiar feature of compressible flows. At large times, the diffusion process, which is qualitatively similar to that of incompressible flows, dominates the entire flow field. The present task is to delineate the flow evolution by means of the matched asymptotic technique with proper timescales.

The paper is organized as follows. The mathematical formulation is stated in § 2. Asymptotic analyses are performed in § 3 for short times and in § 4 for longer diffusive times. In § 5, a stability analysis is conducted to ascertain the feasibility of the solutions. Physical interpretations of the solutions are given in § 6, and comparisons of the present analytical results with numerical solutions are shown. The concluding remarks are summarized in § 7.

2. The problem formulation

In the basic state, a compressible gas in an infinitely long cylindrical pipe of radius R_0, which rotates about the z-axis at constant rotation rate Ω, is in rigid-body rotation. The cylindrical coordinates (r, θ), together with the corresponding velocity components (u, v), are selected, as sketched in figure 1. Both the gas and the pipe wall are assumed to be isothermal at T^*_{00}. For a perfect gas, the density field of this basic state can be expressed as (e.g. Bark & Bark 1976)

$$\rho_{00}[\equiv \rho^*_{00}(r^*)/\rho^*_{00}(R_0)] = \exp\,[\tfrac{1}{2}\gamma M^2(r^2 - 1)]. \tag{1}$$

Superscript $*$ denotes dimensional values and subscript 00 indicates the undisturbed basic state, $M[\equiv \Omega R_0/(\gamma R T^*_{00})^{1/2}]$ the Mach number at the wall, γ the ratio of specific heats of the gas, $r \equiv r^*/R_0$, and R the gas constant. In what follows, it is assumed that $M < 1.0$ and the assumption of the heavy-gas limit is invoked such that γ is set to be $\gamma = 1.0$ (Sakurai & Matsuda 1974; Bark, Meijer & Cohen 1979).

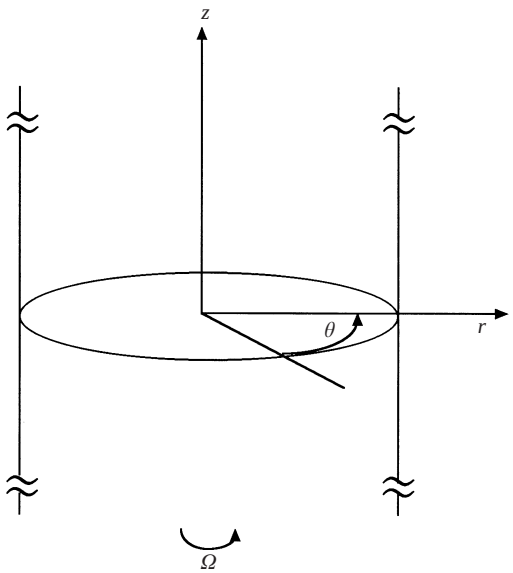

FIGURE 1. Flow configuration and coordinates.

Now, a small perturbation from the basic state is considered. The magnitude of the perturbation is gauged by the Rossby number $\varepsilon \equiv T^p/T^*_{00}$, where T^p is the size of the thermal perturbation in the system. A consistent non-dimensionalization scheme is implemented, as guided by previous studies (e.g. Sakurai & Matsuda 1974; Hultgren, Meijer & Bark 1981):

$$\boldsymbol{u} = (u, v) = \gamma M^2 \boldsymbol{u}^p/\varepsilon\Omega R_0, \quad p = p^p/\varepsilon\rho^*_{00}(R_0)RT^*_{00},$$

$$T = T^p/\varepsilon T^*_{00}, \quad \rho = \rho^p/\varepsilon\rho^*_{00}(R_0), \quad t = t^*\Omega,$$

in which ρ^p, p^p, T^p and $\boldsymbol{u}^p$ represent the dimensional perturbations of density, pressure, temperature and velocity, respectively.

The non-dimensional governing time-dependent compressible-fluid Navier–Stokes equations, written in the cylindrical frame rotating at Ω, are (e.g. Sakurai & Matsuda 1974):

$$M^2\frac{\partial\rho}{\partial t} + \frac{1}{r}\frac{\partial}{\partial r}(r\rho_{00}\,u) = 0, \tag{2}$$

$$\rho_{00}\left(\frac{\partial u}{\partial t} - 2v\right) - M^2 r\rho = -\frac{\partial p}{\partial r} + E\left[\left(\nabla^2 - \frac{1}{r^2}\right)u + \left(\frac{1}{3} + \bar{\beta}\right)\frac{\partial}{\partial r}(\nabla\cdot\boldsymbol{u})\right], \tag{3}$$

$$\rho_{00}\left(\frac{\partial v}{\partial t} + 2u\right) = E\left(\nabla^2 - \frac{1}{r^2}\right)v, \tag{4}$$

$$\rho_{00}\sigma\frac{\partial T}{\partial t} = E\nabla^2 T, \tag{5}$$

$$p = \rho + \rho_{00}\,T. \tag{6}$$

In the above, $\bar{\beta}$ in (3) denotes the ratio of the expansion and shear viscosities, the Prandtl number $\sigma \equiv \mu C_p/k$, μ the coefficient of viscosity, C_p the specific heat at constant pressure, k the coefficient of thermal conductivity, and the Ekman number $E \equiv \mu/[\rho^*_{00}(R_0)\Omega R_0^2]$.

In the present paper, the perturbation, which drives the fluid motion, is assumed to be a change in the wall temperature, T_w. Accordingly, the initial and boundary conditions are stipulated as

$$u = v = T = \rho = 0 \quad \text{at} \quad t = 0, \tag{7a}$$

and

$$u(t, r = 1) = 0, \quad v(t, r = 1) = 0, \quad T(t, r = 1) = T_w. \tag{7b}$$

3. Asymptotic analysis for short times $t \sim O(E^{-1/2})$

For a general discussion of rapidly rotating compressible-fluid flows, it is necessary to examine the early-time behaviour, which is shorter than the diffusive time [$t \sim O(E^{-1})$]. This corresponds to the stage when the thermal front, initiated by the sidewall temperature change, is still close to the wall. Time is scaled as $\tau = E^{-m}t$, $0 < m < 1$. In view of consistent scalings, the dependent variables are expanded in powers of $E^{(1-m)/2}$. In the ensuing discussion, without loss of generality, m is set to be $1/2$ because any choice of m gives the same leading-order equation. The present analysis employs the matched asymptotic method, and the results will show that the boundary layers are coupled to the interior core.

3.1. *Boundary-layer solution*

A stretched radial coordinate $\eta = (1 - r)/E^{1/4}$ is introduced. Expansions are made in the form

$$\varphi^B(\tau, \eta) = \sum_{n=0}^{\infty} \varphi_n^B(\tau, \eta) E^{n/4},$$

in which φ stands for u, v, T, ρ or p, and superscript B denotes the boundary-layer variables.

Upon substituting the expansions into the governing equations, the leading-order equations are

$$M^2 \frac{\partial \rho_0^B}{\partial \tau} - \frac{\partial u_3^B}{\partial \eta} = 0, \tag{8}$$

$$2v_0^B + M^2 \rho_0^B + \frac{\partial p_1^B}{\partial \eta} = 0, \tag{9}$$

$$\frac{\partial v_0^B}{\partial \tau} = \frac{\partial^2 v_0^B}{\partial \eta^2}, \tag{10}$$

$$\sigma \frac{\partial T_0^B}{\partial \tau} = \frac{\partial^2 T_0^B}{\partial \eta^2}, \tag{11}$$

$$\rho_0^B + T_0^B = 0. \tag{12}$$

As seen in (10) and (11), in the initial time of $O(E^{-1/2})$ after the perturbation is imposed impulsively on the wall, the diffusion process progresses over the distance $O(E^{1/4})$ for the azimuthal velocity and temperature. In the light of the initial and boundary conditions of (7), the solutions of (10) and (11) are easily obtained:

$$v_0^B(\tau, \eta) = 0, \tag{13a}$$

$$T_0^B(\tau, \eta) = T_w \operatorname{erfc}(\eta / 2\sqrt{\tau/\sigma}). \tag{13b}$$

For the leading-order density field, (8) and (12) yield

$$u_3^B(\tau,\eta) = \frac{M^2 T_w}{\sqrt{\pi\sigma\tau}} \exp\left(-\frac{\sigma\eta^2}{4\tau}\right), \tag{13c}$$

$$\rho_0^B(\tau,\eta) = -T_w \mathrm{erfc}(\eta/2\sqrt{\tau/\sigma}). \tag{13d}$$

These describe the leading-order variables in the boundary layer. The analysis proceeds to tackle the interior region.

3.2. *Interior solution*

As pointed out previously, over the early-time duration $t \sim O(E^{-1/2})$, the diffusion is significant only in a narrow zone of thickness $O(E^{1/4})$ adjacent to the wall, and the diffusion effect can be neglected in the interior region $0 \leqslant r \leqslant [1 - O(E^{1/4})]$. For the interior region, therefore, the length is scaled as $r \sim O(1)$, and expansions, $\varphi^I(\tau,r) = \sum_{n=0}^{\infty} \varphi_n^I(\tau,r)E^{n/4}$, are carried out for the variables, denoted by superscript I. Then, the leading-order equations are

$$M^2 \frac{\partial \rho_1^I}{\partial \tau} + \frac{1}{r}\frac{\partial (r\rho_{00} u_3^I)}{\partial r} = 0, \tag{14}$$

$$-2\rho_{00} v_1^I - M^2 r \rho_1^I + \frac{\partial p_1^I}{\partial r} = 0, \tag{15}$$

$$\frac{\partial v_1^I}{\partial \tau} + 2u_3^I = 0, \tag{16}$$

$$\rho_{00}\sigma \frac{\partial T_1^I}{\partial \tau} = 0, \tag{17}$$

$$p_1^I = \rho_1^I + \rho_{00} T_1^I. \tag{18}$$

The above equations satisfy the initial conditions $v_T^I = p_1^I = \rho_1^I = T_1^I = 0$. Furthermore, an inspection of (17) and (18) leads to

$$T_1^I = 0, \tag{19a}$$

and

$$\rho_1^I = p_1^I. \tag{19b}$$

Combining (15) and (19*b*) produces

$$v_1^I = \frac{1}{2\rho_{00}}\left[-M^2 r p_1^I + \frac{\partial p_1^I}{\partial r}\right]. \tag{19c}$$

From (14), (16) and (19), a single equation for pressure is obtained:

$$\frac{\partial^2 p_1^I}{\partial r^2} + \left(\frac{1}{r} - M^2 r\right)\frac{\partial p_1^I}{\partial r} - 6M^2 p_1^I = 0. \tag{20}$$

The associated boundary conditions for (20) are

$$\partial p_1^I/\partial r = 0 \quad \text{at} \quad r = 0, \tag{21a}$$

and, from the condition that $u = u_3^I(\tau, r \to 1) + u_3^B(\tau, \eta \to 0) = 0$ at $r = 1$, one has

$$-M^2 p_1^I + \frac{\partial p_1^I}{\partial r} = \frac{8M^2 T_w \sqrt{\tau}}{\sqrt{\pi\sigma}}. \tag{21b}$$

Also, from the condition of total mass conservation $\int_0^1 r\rho \mathrm{d}r = 0$, one finds

$$\int_0^1 r p_1^I \mathrm{d}r = \frac{2T_w\sqrt{\tau}}{\sqrt{\pi\sigma}}. \tag{21c}$$

From (20), by employing an expansion of the form $p_1^I(r,\tau) = \sum_{n=0}^{\infty} M^{2n} p_{1(n)}^I(r,\tau)$, all orders of the complete series solution can be found, i.e.

$$\frac{\partial^2 p_{1(0)}^I}{\partial r^2} + \frac{1}{r}\frac{\partial p_{1(0)}^I}{\partial r} = 0, \tag{22a}$$

$$\frac{\partial^2 p_{1(n)}^I}{\partial r^2} + \frac{1}{r}\frac{\partial p_{1(n)}^I}{\partial r} = r\frac{\partial p_{1(n-1)}^I}{\partial r} + 6p_{1(n-1)}^I \quad (n \geqslant 1). \tag{22b}$$

With the aid of (21), the solutions to (22) up to the third order can be found:

$$p_{1(0)}^I(r,\tau) = \frac{4T_w\sqrt{\tau}}{\sqrt{\pi\sigma}}, \tag{23a}$$

$$p_{1(1)}^I(r,\tau) = \frac{T_w\sqrt{\tau}}{\sqrt{\pi\sigma}}(6r^2 - 3), \tag{23b}$$

and

$$p_{1(2)}^I(r,\tau) = \frac{T_w\sqrt{\tau}}{\sqrt{\pi\sigma}}\left(\frac{12}{5}r^5 - 3r^3 + \frac{18}{35}\right). \tag{23c}$$

The higher-order solutions can, in principle, be obtained by using a recursive procedure from (21) and (22).

Combining the above developments, the uniformly convergent solutions for the interior region in the early stage, in response to the step-change perturbation in the wall temperature, can be written as

$$v_1^I = \frac{T_w\sqrt{\tau}}{\rho_{00}\sqrt{\pi\sigma}}\{M^2(4r) + M^4(6r^4 - 3r^3 - 3r)\} + O(M^6), \tag{24a}$$

$$u_3^I = \frac{-T_w}{4\rho_{00}\sqrt{\pi\sigma\tau}}\{M^2(4r) + M^4(6r^4 - 3r^3 - 3r)\} + O(M^6), \tag{24b}$$

$$\rho_1^I = p_1^I = \frac{T_w\sqrt{\tau}}{\sqrt{\pi\sigma}}\{4 + M^2(6r^2 - 3) + M^4(12r^5/5 - 3r^3 + 18/35)\} + O(M^6), \tag{24c}$$

and

$$T_1^I = 0. \tag{24d}$$

As is evident in the equations, for the early times up to $t \sim O(E^{-1/2})$, the azimuthal velocity and density are $O(E^{1/4})$. Specifically, in the case of an impulsive heating (cooling) of the pipe wall, the resulting azimuthal velocity in the interior increases (decreases). The physical rationalizations may be stated as follows. If a sudden heating (cooling) is applied to the pipe wall, the fluid in the vicinity of the wall expands (shrinks), which generates a radially inward (outward) flow in the interior region. This, in turn, causes the azimuthal velocity to increase (decrease) due to the conservation of angular momentum in the interior region. Concomitantly, the density increases (decreases) since compression (expansion) is achieved by the radially inward (outward) fluid motion. In summary, an impulsive thermal loading at the pipe wall gives rise to an interior fluid motion of magnitude $O(E^{1/4})$.

4. Asymptotic solution at large times $t \sim O(E^{-1})$

To delineate the behaviour on a diffusive timescale, time is scaled $\tau_1 = Et$. Also, for a meaningful problem formulation, appropriate scalings are introduced, i.e. $u \sim O(E)$, $v \sim O(1)$, $T \sim O(1)$, $\rho \sim O(1)$, $p \sim O(1)$ (Sakurai & Matsuda 1974; Bark & Bark 1976). Then, the leading-order equations are

$$M^2 \frac{\partial \rho}{\partial \tau_1} + \frac{1}{r} \frac{\partial (r \rho_{00} u)}{\partial r} = 0, \tag{25a}$$

$$-2\rho_{00} v - M^2 r \rho = -\frac{\partial p}{\partial r}, \tag{25b}$$

$$\rho_{00} \frac{\partial v}{\partial \tau_1} + 2\rho_{00} u = \left(\nabla^2 - \frac{1}{r^2} \right) v, \tag{25c}$$

$$\rho_{00} \sigma \frac{\partial T}{\partial \tau_1} = \nabla^2 T, \tag{25d}$$

$$p = \rho + \rho_{00} T, \tag{25e}$$

where $\rho_{00} = \exp\left(-\frac{1}{2} M^2 (r^2 - 1)\right)$.

Under the constraint that $M < 1.0$, the system of (25) can be tackled by use of the standard series expansion technique. The attendant initial and boundary conditions are re-stated:

$$\left.\begin{aligned} T(r, \tau_1 = 0) = 0, \quad v(r, \tau_1 = 0) = 0, \\ T(r = 1, \tau_1) = T_w, \quad v(r = 1, \tau_1) = 0. \end{aligned}\right\} \tag{26}$$

For example, in order to solve (25*d*), the temperature is decomposed into

$$T = T_w \left[1 + \sum_{n=1}^{\infty} \exp\left(-\beta_n^2 \tau_1 / \sigma\right) T_n(r) \right] + T_w M^2 \sum_{n=1}^{\infty} F_n(r, \tau_1), \tag{27a}$$

and T_n, F_n and β_n are expanded in powers of M^2:

$$T_n = T_{n0} + M^2 T_{n1} + M^4 T_{n2} + \cdots, \tag{27b}$$

$$F_n = F_{n1} + M^2 F_{n2} + \cdots, \tag{27c}$$

$$\beta_n = \beta_{n0} + M^2 \beta_{n1} + M^4 \beta_{n2} + \cdots. \tag{27d}$$

Substitution of (27) into (25*d*) produces a sequence of ordered equations, which leads to a well-posed Sturm–Liouville-type problem.

(i) *The zeroth-order solution*

Combining (25*d*), (26) and (27), one finds

$$\frac{\mathrm{d}^2 T_{n0}}{\mathrm{d}r^2} + \frac{1}{r} \frac{\mathrm{d} T_{n0}}{\mathrm{d}r} + \beta_{n0}^2 T_{n0} = 0, \tag{28a}$$

$$T_{n0}(1) = 0 \quad \text{and} \quad \sum_{n=1}^{\infty} T_{n0}(r) = -1. \tag{28b}$$

The solution of the above equation is readily found:

$$T_{n0}(r) = a_{n0} J_0(r \beta_{n0}), \tag{29}$$

in which a_{n0} is a coefficient to be determined by using (28b), i.e.

$$a_{n0} = \frac{-2}{\beta_{n0} J_1(\beta_{n0})},$$

and β_{n0} is the nth positive zero of $J_0(x)$.

(ii) *The first-order solution*

The function $F_{n1}(r, \tau_1)$ is shown to satisfy the following diffusion equation:

$$\sigma \frac{\partial F_{n1}}{\partial \tau_1} = \nabla^2 F_{n1}. \tag{30a}$$

The initial and boundary conditions to (30a) can be derived by considering (26) and (27):

$$F_{n1}(r, \tau_1 = 0) = 0, \tag{30b}$$

and

$$F_{n1}(r = 1, \tau_1) = -\exp(-\beta_{n0}^2 \tau_1/\sigma) T_{n1}(1), \tag{30c}$$

in which T_{n1} is to be determined later.

From (25d), (26), (27) and (30), the first-order equation reduces to

$$\frac{\mathrm{d}^2 T_{n1}}{\mathrm{d}r^2} + \frac{1}{r}\frac{\mathrm{d}T_{n1}}{\mathrm{d}r} + \beta_{n0}^2 T_{n1} = -2\beta_{n0}\beta_{n1} T_{n0} + \frac{(1-r^2)}{2}\beta_{n0}^2 T_{n0}, \tag{31a}$$

and

$$\sum_{n=1}^{\infty} T_{n1}(r) = 0. \tag{31b}$$

The solution to (31) can be constructed as

$$T_{n1}(r) = A_{n1} J_0(r\beta_{n0}) + B_{n1} r^3 J_1(r\beta_{n0}) + C_{n1} r^2 J_0(r\beta_{n0}), \tag{32}$$

in which the constants A_{n1}, B_{n1}, C_{n1} and β_{n1} are to be determined in view of (31b):

$$\beta_{n1} = \frac{\beta_{n0}}{4} + \frac{1}{6\beta_{n0}},$$

$$\begin{aligned} A_{n1} &= \frac{-2}{J_1^2(\beta_{n0})} \int_0^1 r J_0(r\beta_{n0}) \sum_{k=1}^{\infty} (B_{k1} r^3 J_1(r\beta_{k0}) + C_{k1} r^2 J_0(r\beta_{k0}))\mathrm{d}r \\ &= \frac{1}{J_1(\beta_{n0})}\left(\frac{1}{3\beta_{n0}^3} - \frac{1}{6\beta_{n0}}\right) + \frac{\beta_{n0}}{J_1(\beta_{n0})} \sum_{\substack{k=1 \\ (k\neq n)}}^{\infty} \left\{\frac{4\beta_{k0}^2}{(\beta_{n0}^2 - \beta_{k0}^2)^3} - \frac{1}{3(\beta_{n0}^2 - \beta_{k0}^2)}\right\}, \end{aligned}$$

$$B_{n1} = \frac{1}{6J_1(\beta_{n0})},$$

$$C_{n1} = \frac{1}{6\beta_{n0} J_1(\beta_{n0})}.$$

The formal solution of the cylindrical diffusion equation, (30)–(32), is a classical

one (e.g. Carslaw & Jaeger 1959, pp. 198–200):

$$F_{n1}(r,\tau_1) = -\frac{1}{3\sigma}\exp(-\beta_{n0}^2\tau_1/\sigma)\frac{\tau_1\beta_{n0}J_0(r\beta_{n0})}{J_1(\beta_{n0})} + \frac{1}{3}\sum_{\substack{k=1\\(k\neq n)}}^{\infty}\frac{\beta_{k0}}{(\beta_{n0}^2-\beta_{k0}^2)}\frac{J_0(r\beta_{k0})}{J_1(\beta_{k0})}$$

$$\times\left[\exp\left(-\frac{\beta_{n0}^2}{\sigma}\tau_1\right)-\exp\left(-\frac{\beta_{k0}^2}{\sigma}\tau_1\right)\right]. \tag{33}$$

Summarizing the analytical developments, the solution for temperature is expressed as

$$T(r,\tau_1) = T^{(0)} + M^2T^{(1)} + O(M^4),$$

where

$$T^{(0)} = T_w\left[1-2\sum_{n=1}^{\infty}\exp\left(-\frac{\beta_{n0}^2\tau_1}{\sigma}\right)\frac{J_0(r\beta_{n0})}{\beta_{n0}J_1(\beta_{n0})}\right], \tag{34a}$$

$$T^{(1)} = T_w\sum_{n=1}^{\infty}\left[F_{n1}(r,\tau_1)+\exp\left(-\frac{\beta_{n0}^2\tau_1}{\sigma}\right)\left(T_{n1}(r)-\frac{2\tau_1\beta_{n0}\beta_{n1}}{\sigma}T_{n0}(r)\right)\right]. \tag{34b}$$

As anticipated, the above large-time behaviour is revealing. The zeroth-order solution, as is discernible in (34*a*), represents the straightforward diffusion process, which is the same as for the case of an incompressible fluid. The compressible-fluid effect is embedded in the first-order solution.

The solutions for density, pressure, radial and azimuthal velocities can be found in a similar manner. The dependent variables are expanded as follows:

$$u = u^{(0)} + M^2u^{(1)} + \cdots,$$

$$v = v^{(0)} + M^2v^{(1)} + \cdots,$$

$$\rho = \rho^{(0)} + M^2\rho^{(1)} + \cdots,$$

$$p = p^{(0)} + M^2p^{(1)} + \cdots.$$

One finds, from (25*a*) and (25*c*),

$$u^{(0)} = v^{(0)} = 0. \tag{35}$$

It follows, from (25*b*), that $\partial p^{(0)}/\partial r = 0$, therefore

$$p^{(0)} = f(\tau_1), \tag{36}$$

and

$$\rho^{(0)} = -T^{(0)} + f(\tau_1). \tag{37}$$

In the above, $f(\tau_1)$ is an arbitrary function to be determined by the global mass continuity condition $\int_0^1 \rho r\,\mathrm{d}r = 0$:

$$f(\tau_1) = T_w\left\{1-4\sum_{n=1}^{\infty}\exp\left(-\frac{\beta_{n0}^2\tau_1}{\sigma}\right)\frac{1}{\beta_{n0}^2}\right\}. \tag{38}$$

From (25*a*), $u^{(1)}$ is given by

$$u^{(1)} = \frac{2}{\sigma}T_w\sum_{n=1}^{\infty}\exp\left(-\frac{\beta_{n0}^2}{\sigma}\tau_1\right)\frac{J_1(r\beta_{n0})-rJ_1(\beta_{n0})}{J_1(\beta_{n0})}. \tag{39}$$

The solution $u^{(1)}$ in (39) does not converge to zero as $\tau_1 \to 0$, because u is $O(E^{3/4})$ at $t \sim O(E^{-1/2})$. It is recalled that u is scaled $O(E)$ for $t \sim O(E^{-1})$.

From (25*c*), one can obtain the equation for $v^{(1)}$ and the auxiliary conditions:

$$\frac{\partial v^{(1)}}{\partial \tau_1} + 2u^{(1)} = \left(\nabla^2 - \frac{1}{r^2}\right) v^{(1)}, \tag{40}$$

$$v^{(1)}(\tau_1 = 0, r) = 0 \quad \text{and} \quad v^{(1)} = (\tau_1, r = 0) = 0.$$

The solution to (40) can be found by the Laplace transform method:
In the case of $\sigma = 1$

$$v^{(1)} = 4T_w \sum_{n=1}^{\infty} \left\{ \left(r - \frac{J_1(r\beta_{n0})}{J_1(\beta_{n0})} \right) \tau_1 \exp(-\beta_{n0}^2 \tau_1) + G_n(\tau_1, r) \right\}, \tag{41a}$$

in which

$$G_n = 2 \sum_{k=1}^{\infty} \left\{ \frac{\exp(-\beta_{n0}^2 \tau_1) - \exp(-\gamma_k^2 \tau_1)}{(\gamma_k^2 - \beta_{n0}^2)^2} - \frac{\tau_1 \exp(-\beta_{n0}^2 \tau_1)}{(\gamma_k^2 - \beta_{n0}^2)} \right\} \frac{\beta_{n0}^2 J_1(\gamma_k r)}{\gamma_k J_0(\gamma_k)},$$

and γ_k is the kth positive zero of $J_1(x)$.
In the case of $\sigma \neq 1$

$$v^{(1)} = 4T_w \sum_{n=1}^{\infty} \left\{ \left(r - \frac{J_1(r\beta_{n0})}{J_1(\beta_{n0})} \right) \frac{\exp(-\beta_{n0}^2 \tau_1/\sigma) - \exp(-\beta_{n0}^2 \tau_1)}{(\sigma - 1)\beta_{n0}^2} + H_n(\tau_1, r) \right\}, \tag{41b}$$

in which

$$H_n = \frac{2}{\sigma - 1} \sum_{k=1}^{\infty} \left\{ \frac{\exp(-\beta_{n0}^2 \tau_1) - \exp(-\gamma_k^2 \tau_1)}{\gamma_k^2 - \beta_{n0}^2} \right.$$

$$\left. - \frac{\exp(-\beta_{n0}^2 \tau_1/\sigma) - \exp(-\gamma_k^2 \tau_1)}{\gamma_k^2 - \beta_{n0}^2/\sigma} \right\} \frac{J_1(\gamma_k r)}{\gamma_k J_0(\gamma_k)}.$$

It is an easy exercise to recover the result of (41*a*) by letting $\sigma \to 1$ in (41*b*).

The higher-order solutions may be obtained, in principle, from (25*a*)–(25*e*) in a similar fashion. However, the above leading-order solutions portray the salient flow characteristics in sufficient detail.

5. Stability of the flow

In an effort to evaluate the feasibility of the analytically obtained flow of §§ 3 and 4, the issue of stability, within the specific parameter ranges of present concern, is addressed. For a formal stability analysis, the analytical solution constitutes the basic state, which, in dimensional form, is re-capitulated:

$$u_B^* = \varepsilon E \frac{\Omega R_0}{\gamma M^2} u(\tau, r), \quad v_B^* = \varepsilon \frac{\Omega R_0}{\gamma M^2} v(\tau, r),$$

$$p_B^* = \rho_{00}^*(R_0) R T_{00}^* (\rho_{00}(r) + \varepsilon p(\tau, r)),$$

$$T_B^* = T_{00}^* (1 + \varepsilon T(\tau, r)), \quad \rho_B^* = \rho_{00}^*(R_0)(\rho_{00}(r) + \varepsilon \rho(\tau, r)),$$

where superscript $*$ stands for dimensional variables and subscript B the basic state.

To examine the stability of the above basic-state flow, a small non-dimensional perturbation (denoted by a tilde) is added:

$$u^* = u_B^*(\tau, r) + \frac{\Omega R_0}{\gamma M^2}\tilde{u}(t, r, \theta, z), \tag{42a}$$

$$v^* = v_B^*(\tau, r) + \frac{\Omega R_0}{\gamma M^2}\tilde{v}(t, r, \theta, z), \tag{42b}$$

$$w^* = \frac{\Omega R_0}{\gamma M^2}\tilde{w}(t, r, \theta, z) \tag{42c}$$

$$p^* = p_B^*(\tau, r) + \rho_{00}^*(R_0) R T_{00}^* \tilde{p}(t, r, \theta, z), \tag{42d}$$

$$T^* = T_B^*(\tau, r) + T_{00}^* \tilde{T}(t, r, \theta, z), \tag{42e}$$

$$\rho^* = \rho_B^*(\tau, r) + \rho_{00}^* \tilde{\rho}(t, r, \theta, z), \tag{42f}$$

in which $t \equiv t^* \Omega$ and $\tau \equiv t^* E \Omega$.

Expressions (42) are substituted into the governing compressible Navier–Stokes equations. After undertaking the simplifications pertinent to the assumptions $\gamma \to 1.0$, $\sigma \sim O(1)$, $E \ll 1$, the linearized equations for the stability analysis are obtained:

$$M^2 \frac{\partial \tilde{\rho}}{\partial t} + \varepsilon \frac{v}{r}\frac{\partial \tilde{\rho}}{\partial \theta} + \tilde{u}\frac{\partial \rho_0}{\partial r} + \rho_0 \nabla \cdot \tilde{\boldsymbol{V}} = 0, \tag{43a}$$

$$\rho_0 \left(\frac{\partial \tilde{\boldsymbol{V}}}{\partial t} + \frac{\varepsilon}{M^2}\frac{v}{r}\frac{\partial \tilde{\boldsymbol{V}}}{\partial \theta} + 2\boldsymbol{e}_k \times \tilde{\boldsymbol{V}} \right) - \tilde{\rho}\left(2\varepsilon v + M^2 r + \varepsilon^2 \frac{v^2}{M^2 r} \right) \boldsymbol{e}_r = -\nabla \tilde{p}, \tag{43b}$$

$$\frac{\partial \tilde{p}}{\partial t} + \frac{\varepsilon}{M^2}\frac{v}{r}\frac{\partial \tilde{p}}{\partial \theta} + \frac{\tilde{u}}{M^2}\frac{\partial p_0}{\partial r} - T_0 \left(\frac{\partial \tilde{\rho}}{\partial t} + \frac{\varepsilon}{M^2}\frac{v}{r}\frac{\partial \tilde{\rho}}{\partial \theta} + \frac{\tilde{u}}{M^2}\frac{\partial \rho_0}{\partial r} \right) = 0. \tag{43c}$$

In the above, $\tilde{\boldsymbol{V}}$ indicates the non-dimensional perturbed velocity, $\tilde{\boldsymbol{V}} = \tilde{u}\boldsymbol{e}_r + \tilde{v}\boldsymbol{e}_\theta + \tilde{w}\boldsymbol{e}_z$, $(\boldsymbol{e}_r, \boldsymbol{e}_\theta, \boldsymbol{e}_z)$ the unit vectors in the (r, θ, z)-directions, and p_0, ρ_0 and T_0 denote, respectively, the non-dimensional basic states, i.e. $p_0 = \rho_{00} + \varepsilon p$, $\rho_0 = \rho_{00} + \varepsilon\rho$ and $T_0 = 1 + \varepsilon T$.

To investigate stability, the perturbations in (43) are assumed to be of the form

$$\begin{bmatrix} \tilde{u}(r, \theta, z, t) \\ \tilde{v}(r, \theta, z, t) \\ \tilde{w}(r, \theta, z, t) \\ \tilde{p}(r, \theta, z, t) \\ \tilde{\rho}(r, \theta, z, t) \end{bmatrix} = \begin{bmatrix} \hat{u}(r, \theta, z) \\ \hat{v}(r, \theta, z) \\ \hat{w}(r, \theta, z) \\ \hat{p}(r, \theta, z) \\ \hat{\rho}(r, \theta, z) \end{bmatrix} \exp(\mathrm{i}\omega) = \begin{bmatrix} \bar{u}(r) \\ \bar{v}(r) \\ \bar{w}(r) \\ \bar{p}(r) \\ \bar{\rho}(r) \end{bmatrix} \exp[\mathrm{i}(\omega t - m\theta - kz)], \tag{44}$$

in which $\omega = \omega_r + \mathrm{i}\omega_i$ is the complex frequency, and m and k the real azimuthal and axial wavenumbers.

(*a*) Stability criterion for the case of $\varepsilon \sim O(E)$

Neglecting the $O(E)$-term, the physical properties of the fluid at the basic state are reduced to $T_0 = 1$ and $p_0 = \rho_0 = \rho_{00}$. Consequently, from (43*c*) and (44),

$$\hat{p}(r) = \hat{\rho}(r). \tag{45}$$

The result shown in (45) is in accord with the analysis of § 4 for the inviscid region, which ascertains that the process of physical property variations is isothermal and

isentropic. It is recalled here that the entire analyses represent the leading-order behaviour under the assumption $E \ll 1$.

Placing (44) into (43a) and (43b), together with (45), produces

$$\mathrm{i}\omega M^2 \hat{p} + \rho_{00} M^2 r\hat{u} + \rho_{00} \nabla \cdot \hat{\boldsymbol{V}} = 0, \tag{46a}$$

$$\mathrm{i}\omega \rho_{00} \hat{\boldsymbol{V}} + 2\rho_{00} \boldsymbol{e}_k \times \hat{\boldsymbol{V}} - M^2 r\hat{p}\boldsymbol{e}_r + \nabla \hat{p} = 0, \tag{46b}$$

in which $\hat{\boldsymbol{V}} = \hat{u}\boldsymbol{e}_r + \hat{v}\boldsymbol{e}_\theta + \hat{w}\boldsymbol{e}_z$.

Undergoing a procedure similar to Gans (1974), the complex conjugate of (46a) is taken, and it is integrated over the whole flow domain, after multiplication by $\hat{p}$:

$$-\mathrm{i}\omega^+ M^2 \left\langle \frac{1}{\rho_{00}} \hat{p}\hat{p}^+ \right\rangle + M^2 \langle r\hat{p}\hat{u}^+ \rangle + \langle \hat{p} \nabla \cdot \hat{\boldsymbol{V}}^+ \rangle = 0, \tag{47a}$$

$$\mathrm{i}\omega \langle \rho_{00} \hat{\boldsymbol{V}} \cdot \hat{\boldsymbol{V}}^+ \rangle + 2\langle \rho_{00} \boldsymbol{e}_k \times \hat{\boldsymbol{V}} \cdot \hat{\boldsymbol{V}}^+ \rangle - M^2 \langle r\hat{p}\hat{u}^+ \rangle + \langle \nabla \hat{p} \cdot \hat{\boldsymbol{V}}^+ \rangle = 0. \tag{47b}$$

In the above $+$ and $\langle\ \rangle$ denote, respectively, the complex conjugate and integration $\int_0^1 (\ ) 2\pi r\, \mathrm{d}r$. By adding (47$a$) and (47$b$), and using the boundary condition $\hat{\boldsymbol{V}}^+ \cdot \boldsymbol{n} = 0$ where $\boldsymbol{n}$ denotes outward normal vector, yields

$$\mathrm{i}\omega \langle \rho_{00} \hat{\boldsymbol{V}} \cdot \hat{\boldsymbol{V}}^+ \rangle + 2\langle \rho_{00} \boldsymbol{e}_k \times \hat{\boldsymbol{V}} \cdot \hat{\boldsymbol{V}}^+ \rangle - \mathrm{i}\omega^+ M^2 \left\langle \frac{1}{\rho_{00}} \hat{p}\hat{p}^+ \right\rangle = 0. \tag{48}$$

The vanishing of the real part of the left-hand side of (48),

$$\omega_i \left\{ \langle \rho_{00} \hat{\boldsymbol{V}} \cdot \hat{\boldsymbol{V}}^+ \rangle + M^2 \left\langle \frac{1}{\rho_{00}} \hat{p}\hat{p}^+ \right\rangle \right\} = 0,$$

requires that $\omega_i = 0$. This implies that the basic-state flow, given by the analytically obtained solution of early sections, is stable within the specific parameter ranges of present concern.

(b) Stability criterion for the case of $O(E) \ll \varepsilon < 1$.

The substitution of (44) into (43) produces

$$\mathrm{i}\Lambda\bar{\rho} + \bar{U}\rho_0' + \rho_0 \left[\frac{\mathrm{d}\bar{U}}{\mathrm{d}r} + \frac{\bar{U}}{r} - \frac{\mathrm{i}m}{r}\bar{V} - \mathrm{i}k\bar{W} \right] = 0, \tag{49a}$$

$$\mathrm{i}\rho_0 \Lambda \bar{U} - 2\rho_0 \left(\frac{V_0}{r} + 1 \right) \bar{V} - \bar{\rho} \left(\frac{(V_0)^2}{r} + 2(V_0) + r \right) = -\frac{\mathrm{d}\bar{P}}{\mathrm{d}r}, \tag{49b}$$

$$\mathrm{i}\rho_0 \Lambda \bar{V} + \rho_0((V_0)' + \frac{(V_0)}{r} + 2)\bar{U} = \frac{\mathrm{i}m}{r}\bar{P}, \tag{49c}$$

$$\mathrm{i}\rho_0 \Lambda \bar{W} = \mathrm{i}k\bar{P}, \tag{49d}$$

$$\mathrm{i}\Lambda\bar{P} + \bar{u}P_0' = C_0^2(\mathrm{i}\Lambda\bar{\rho} + \bar{U}\rho_0'), \tag{49e}$$

in which $V_0 = \varepsilon M^{-2} v$, $P_0 = p_0/M^2$, $\Lambda = \omega - m(V_0)/r$, $(\bar{U}, \bar{V}, \bar{W}) = M^2(\bar{u}, \bar{v}, \bar{w})$, $C_0^2 = T_0/M^2$ and the prime denotes differentiation with respect to r.

Equations (49a)–(49e) are identical to (2.11)–(2.15) of the paper by Lalas (1975) which studied the stability of compressible swirling flows. It is noted that, in Lalas (1975), $\sigma = 1$ (angular velocity of the pipe), and $W = 0$ (basic axial velocity). By undertaking steps analogous to the analysis of Lalas, the stability criterion emerges: the sufficient condition for stability is reduced to $R_i \geqslant 1/4$, where R_i is the effective

Richardson number

$$R_i = N^2 \Big/ \left(\frac{\mathrm{d}V_0}{\mathrm{d}r} - \frac{V_0}{r}\right)^2.$$

In the above the effective Brunt–Väisälä frequency N is introduced,

$$N = \left[\left(\frac{\rho_0'}{\rho_0} - \frac{P_0'}{\rho_0 C_0^2}\right)\frac{(V_0 + r)^2}{r}\right]^{1/2}.$$

The details of mathematical manipulations can be found in Lalas (1975). In summary, in the present analysis, for small but finite Rossby number $O(E) \ll \varepsilon < O(1)$, the basic-state flow is shown to be stable when the condition $R_i \geqslant 1/4$ is satisfied.

The principal findings of the foregoing stability analysis are summarized. When the thermal perturbation at the wall is very small, $\varepsilon \sim O(E)$, the flow is absolutely stable. In this case, the above theoretical solution represents a physically feasible flow.

When the perturbation at the wall is small but finite, $O(E) \ll \varepsilon < 1$, a further consideration is in order. For small values of Mach number, the Richardson number can be approximated as

$$R_i \approx C_r \varepsilon^{-1} + O(M^4),$$

in which

$$C_r \equiv -\frac{(T'^{(0)} + M^2 \rho_{00} T'^{(1)})}{r^3 \rho_{00}} \left[\frac{1}{r + M^2 v^{(1)}} \frac{\mathrm{d}(v^{(1)}/r)}{\mathrm{d}r}\right]^{-2},$$

where $T^{(0)}$, $T^{(1)}$ and $v^{(1)}$ are given in (34*a*), (34*b*) and (41), respectively. The variations of these functions with time are plotted in figures 5, 6 and 7 in § 6.3. It is observed that, when the wall is heated, i.e. $T_w > 0$, $T'^{(0)} + M^2 \rho_{00} T'^{(1)} > 0$, pointing to $R_i < 0$, which implies instability (see figures 5, 6*c* and 7*c*). On the other hand, when the wall is cooled, i.e. $T_w < 0$, it is seen that $T'^{(0)} + M^2 \rho_{00} T'^{(1)} < 0$. Based on these arguments, the parameter ranges for the sufficient condition for stability, $R_i \geqslant 1/4$, can be found:

$$0 \leqslant \varepsilon \leqslant \min_{0 \leqslant r \leqslant 1} \{C_r(r)\} + O(M^4).$$

As emphasized previously, the major thrust of this paper concerns the transient behaviour of a physically feasible flow. Detailed and in-depth discussions on the stability issues are beyond the scope of this paper. In conclusion, the present analytical solution represents a physically realizable flow when $\varepsilon \sim O(E)$. When $O(E) \ll \varepsilon < 1$, the applicability of the present solution is restricted to the case when $T_w < 0$ and in a limited range of ε as shown above.

6. Results and discussion

6.1. *Comparisons with the numerical solution*

Before proceeding further, a numerical solution for the temperature field has been obtained to verify the analytical results. In order to solve numerically the temperature equation (5), an explicit scheme is adopted:

$$\sigma \exp\left[-\tfrac{1}{2}M^2(r_j^2 - 1)\right][T_j^{n+1} - T_j^n] = E(\Delta t)[(T_{j+1}^n - 2T_j^n + T_{j-1}^n)/(\Delta r)^2 + (T_{j+1}^n - T_{j-1}^n)/(2r_j \Delta r)],$$

where superscript n denotes the time step and subscript j the spatial grid point. For the calculations, 201 uniformly spaced grid points ($\Delta r = 0.005$), together with the time step $E\Delta t = 10^{-5}$, were used.

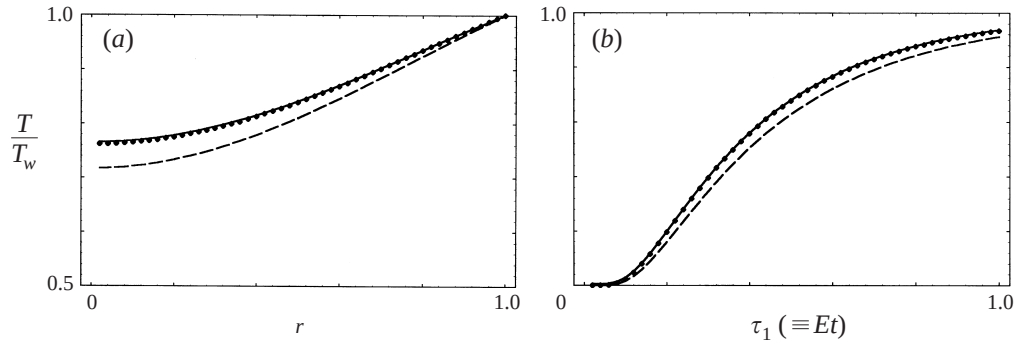

FIGURE 2. Comparison between the present analytic solution and the full numerical solution. (*a*) Temperature profile at $\tau_1(\equiv E^{-1}t) = 0.3$. (*b*) Evolution of temperature at $r = 0.5$. $M = 0.5$ and $\sigma = 1.0$. ●, numerical solution; – – –, $T^{(0)}$ from (34*a*); ——, $T^{(0)} + M^2\,T^{(1)}$ from (34*a*) and (34*b*).

Comparisons between the numerical solutions and the analytical solutions are given in figure 2 for $M = 0.5$. The temperature profile at $t = 0.3$ is shown in figure 2(*a*), and the temperature evolution at $r = 0.5$ in figure 2(*b*). The analytical series solutions were computed by summing to the 100th term. As is evident, the analytical solution, which contains the zeroth and first terms [$T \equiv T^{(0)} + M^2 T^{(1)}$], is in broad agreement with the full numerical solution. This establishes the accuracy and robustness of the present analytical solution procedures for both the early-time and large-time stages. As stressed earlier, the crux lies in the differences between the compressible- and incompressible-fluid behaviour.

6.2. *Short-time behaviour for* $t \sim O(E^{-1/2})$

The radial profiles of flow variables in the early stage near the wall are illustrated in figure 3. The temperature variations cause alterations in the density field, and these result in volume changes near the wall. Therefore, flows are induced in the radial direction, which are apparent in the plots of figure 3. This evolutionary process is characteristic of compressible-fluid flows.

The evolution of azimuthal velocity v in the interior is exhibited in figure 4(*a*). As seen in figure 4(*a*), the strength of v is $O(E^{1/4})$ in the early phase $t \sim O(E^{-1/2})$. If an impulsive heating (cooling) is applied to the wall (which corresponds to a positive (negative) T_w), the fluid in the immediate vicinity of the wall expands (shrinks). This causes the afore-mentioned radially inward (outward) motion in the bulk flow field. Since the interior region is essentially inviscid, angular momentum is conserved. Consequently, the above-described radially inward (outward) flow causes the azimuthal velocity to increase (decrease) accordingly. The overall pictures of figures 3 and 4(*a*) are consistent with the above physical rationalization. In figure 4(*a*), the magnitude of v is seen to increase as the Mach number M increases or the Prandtl number σ decreases. This is anticipated in the light of the fact that the thermally driven fluid expansion (or compression) is more effective at larger M or lower σ.

The evolution of radial velocity u in the interior is displayed in figure 4(*b*). Clearly, the heating (cooling) at the wall induces a radially inward (outward) motion. The radial flow intensifies as M increases or σ decreases, which is in accord with the result for v. As time elapses toward $t \sim O(E^{-1/2})$, the induced radial flow diminishes, as shown in figure 4(*b*). The evolution of density in the interior is depicted in figure

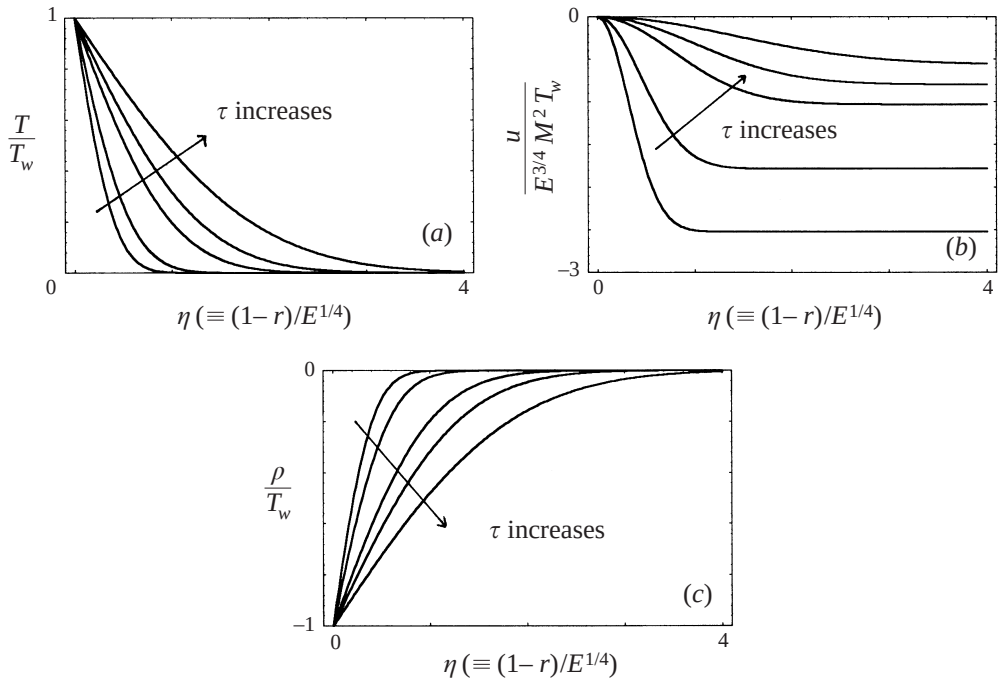

FIGURE 3. Profiles of temperature (*a*), radial velocity (*b*) and density (*c*) near the wall at early times. $M = 0.3$ and $\sigma = 1.0$. Times, $\tau \equiv E^{1/2}t$, are 0.05, 0.1, 0.3, 0.5, 1.0.

4(*c*). The radially inward (outward) motion causes the interior density to increase (decrease).

As can be inferred from (19*a*) and (19*b*), the above-described motion in the interior is essentially isothermal and isentropic, i.e.

$$T \approx O(E^{1/2}) \quad \text{and} \quad p \approx \rho + O(E^{1/2}). \tag{50}$$

It is recalled that, for an isentropic process, $p \sim \rho^r$, from which (50) is recovered in the limit $\gamma \to 1$ and $E \to 0$. Physically, it can be argued that, in the heavy-gas limit ($\gamma \to 1$) and for very small Ekman number, the thermal perturbation at the wall propagates thermo-acoustically into the interior toward the axis as a compression (expansion) wave for a positive (negative) T_w. The propagation speed is equal to the acoustic velocity. The implication, therefore, is that there exists an additional characteristic timescale of $O(M)$, which is much shorter than the principal timescale of present concern, $O(E^{-1/2})$ (see e.g. Spradley & Churchill 1975; Ozoe, Sato & Churchill 1980; Hyun & Park 1989). This also explains why the radial velocity u in figure 4(*b*) does not converge to zero as $\tau \to 0$. A far more thorough analysis, introducing a shorter timescale $O(M)$, will be required to depict the thermo-acoustic wave. This is not pursued in the present paper, since the impact of thermo-acoustic phenomenon is small on the longer-time behaviour over $t \sim O(E^{-1/2})$ or $t \sim O(E^{-1})$ (see Ozoe *et al.* 1980; Hyun & Park 1989; Park & Hyun 1989).

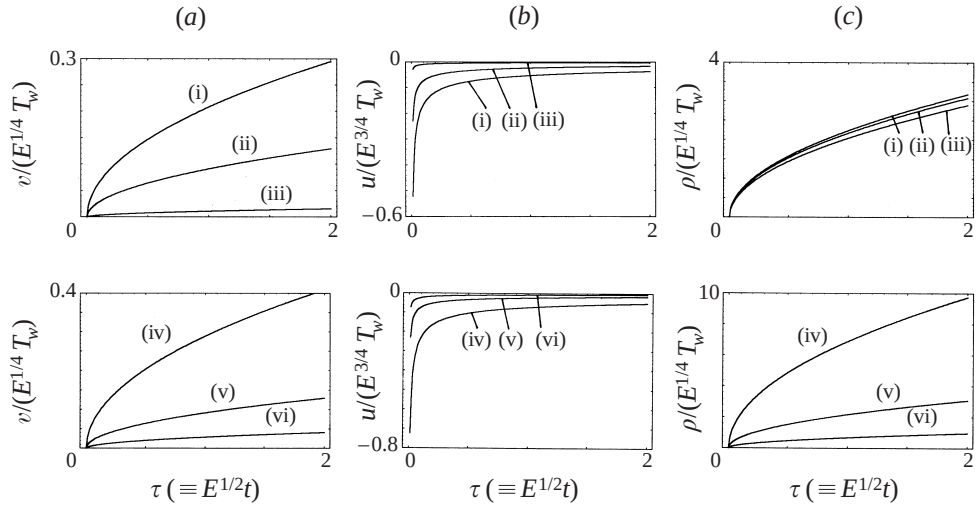

FIGURE 4. Interior azimuthal velocity $v(a)$, radial velocity $u(b)$ and density $\rho(c)$ with time τ. The radial position, r, is 0.5. In the top frames, the Mach numbers, M, are (i) 0.5; (ii) 0.3; (iii) 0.1. $\sigma = 1.0$. In the bottom frames, the Prandtl numbers, σ, are (iv) 0.1; (v) 1.0; (vi) 10.0. $M = 0.3$.

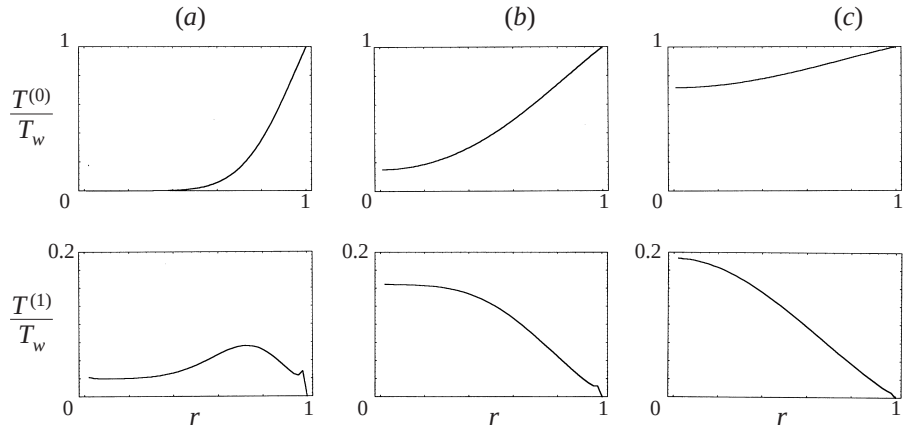

FIGURE 5. Temperature field at large times over the diffusion timescale. The top frames show $T^{(0)}$, and the bottom frames $T^{(1)}$. $\sigma = 1.0$. (*a*) $\tau_1[\equiv Et] = 0.1$, (*b*) $\tau_1 = 0.3$, (*c*) $\tau_1 = 0.5$.

6.3. *Long-time behaviour for* $t \sim O(E^{-1})$

The series solutions at large times, elaborated in § 4, are computed by summing to the 100th term.

The profiles of temperature are illustrated in figure 5. The lowest-order solution, $T^{(0)}$ in (34*a*), and the first-order solution, $T^{(1)}$ in (34*b*), are plotted. As clearly demonstrated, $T^{(0)}$ is exactly the solution to the diffusion equation, which is the case of an incompressible fluid. The compressibility effect is contained in the first-order and higher-order solutions. As time $\tau_1[\equiv Et]$ progresses, the region of substantial values of $T^{(1)}$ is shifted from large radii to the entire flow field. As can be understood from (25*d*), with the aid of the compressibility effect, the transitory time to reach steady state is shortened. As M increases, the effective diffusion coefficient increases,

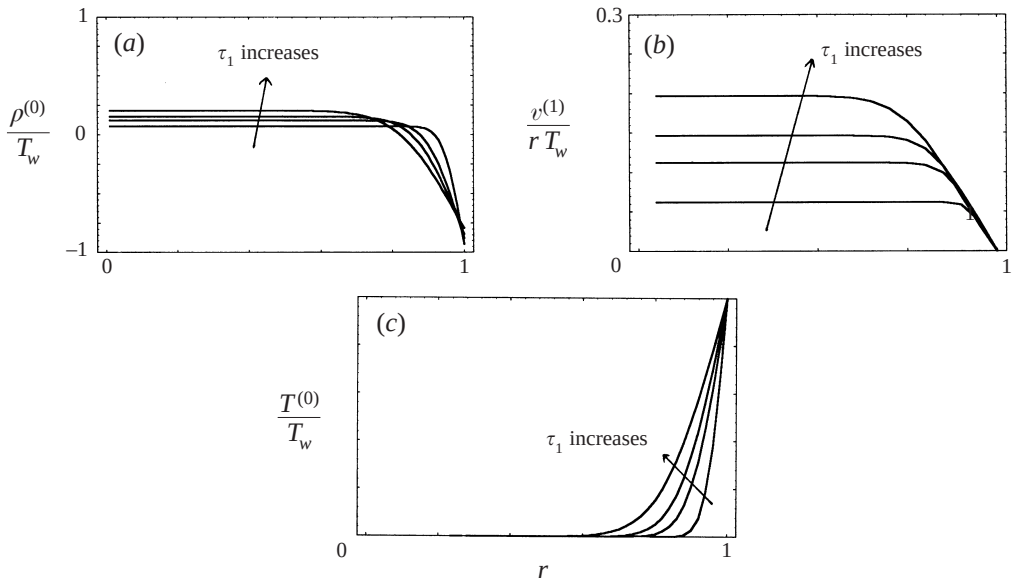

FIGURE 6. Profiles of density $\rho^{(0)}$ (*a*), angular velocity $v^{(1)}/r$ (*b*) and temperature $T^{(0)}$ (*c*) in the initial stage. $\sigma = 1.0$. Times, $\tau_1 \equiv Et$, are 0.001, 0.003, 0.005, 0.009.

which facilitates the thermal diffusion process. These observations are consistent with the previous theoretical findings (e.g. Bark & Bark 1976; Park & Hyun 1997, 1998).

The radial profiles of leading-order density, $\rho^{(0)}$, angular velocity, $v^{(1)}/r$, and temperature, $T^{(0)}$, which are respectively calculated by using (37), (41*a*) and (34*a*), are now described. Figure 6 exhibits the flow variables at very small times. The plots in figure 6(*a*) demonstrate that, after a positive (negative) thermal impact is imposed at the wall, a compression (expansion) of the inner interior fluid and an expansion (compression) of the fluid near the wall take place. Inspection of figures 6(*a*) and 6(*c*) reveals that these two regions are separated by a narrow zone of steep temperature gradients, which will be termed the thermal front. The plots of angular velocity of figure 6(*b*) similarly point to the division of the entire flow field into two regions: the inner inviscid region at small radii and the outer viscous region at larger radii. As remarked earlier, in the inner region, the isothermal–isentropic relation ($p^{(0)} = \rho^{(0)}$) prevails for $t \sim O(E^{-1})$. This implies that, at a given location in the inner region, the initial angular momentum is conserved until this location is engulfed by the approaching thermal front and the thermo-acoustic disturbance propagates. Therefore, at a location in the inviscid inner region, by the imposition of a positive (negative) T_w at the wall, the spin-up (spin-down) process progresses through the radially inward (outward) fluid motion until the thermal front reaches this location. This process is akin to the conventional mechanically driven spin-up of an incompressible fluid in a confined cylinder with rotating disks (Greenspan & Howard 1963). However, an important difference should also be noted. For the conventional spin-up, the radial motion is generated by the Ekman layer pumping at the disk. In the present problem, the radial flow is initiated by thermal expansion of the fluid in the outer viscous region. The angular velocity in the inviscid inner region is uniform, and its magnitude increases as time elapses. Obviously, in the outer viscous region, angular momentum is not conserved, and the angular velocity falls to zero as the radial position moves toward the wall.

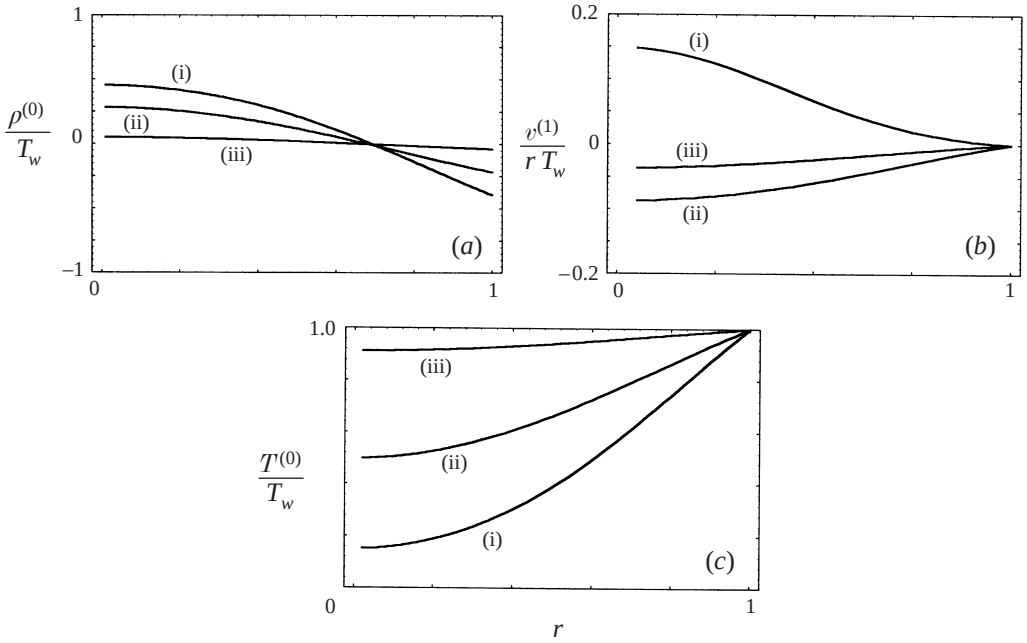

FIGURE 7. Profiles of density $\rho^{(0)}$ (*a*), angular velocity $v^{(1)}/r$ (*b*) and temperature $T^{(0)}$ (*c*) in the intermediate phase. $\sigma = 1.0$. Times, $\tau_1 \equiv Et$, are (i) 0.1; (ii) 0.2; (iii) 0.5.

The flow behaviour at a large time, i.e. after the thermal front has reached the rotating axis, is depicted in figure 7. (The ensuing discussion is for $T_w > 0$.) Immediately after the arrival of the front at the axis (see curves (i) in figure 7), the temperature near the axis does not deviate much from the initial-state value. However, the temperature increases with r, and it reaches the value imposed at the wall. Accordingly, the density decreases at large radii. The angular velocity is higher at small radii since the radially inward motion is sustained over a longer time. Alternatively stated, the fluid near the rotation axis has undergone the inviscid spin-up process over a longer period than the fluid at large radii (see curve (i) in figure 7(*b*)).

After the thermal front has reached the axis, the entire flow field is influenced by the viscous effect, and diffusion of angular momentum takes place. Consequently, the conservation of angular momentum is not sustained in the whole flow field. The implication is that the attenuation of angular momentum is comparatively larger in the near-axis region since the absolute magnitude of angular velocity was relatively large there. By means of thermal diffusion, in the near-axis region, the temperature increases, and, concomitantly, volume expansion of the fluid occurs, which generates a radially outward motion. Therefore, for the fluid at large radii near the wall, the density had been decreased previously by the expansion due to the initial imposition of T_w at the wall. However, the fluid at large radii is compressed this time by the previously described radially outward flow. At first glance, this compression at large radii appears to be similar to the compression of the near-axis fluid by the early-time radially inward propagation of the thermal front. However, a significant difference is stressed. The early-time compression of the inner interior fluid is basically an inviscid, isothermal–isentropic process; thus, the angular momentum is conserved. On the other hand, the compression of the near-wall fluid at large times is a viscously controlled diffusion process, in which the angular momentum is not conserved. This latter

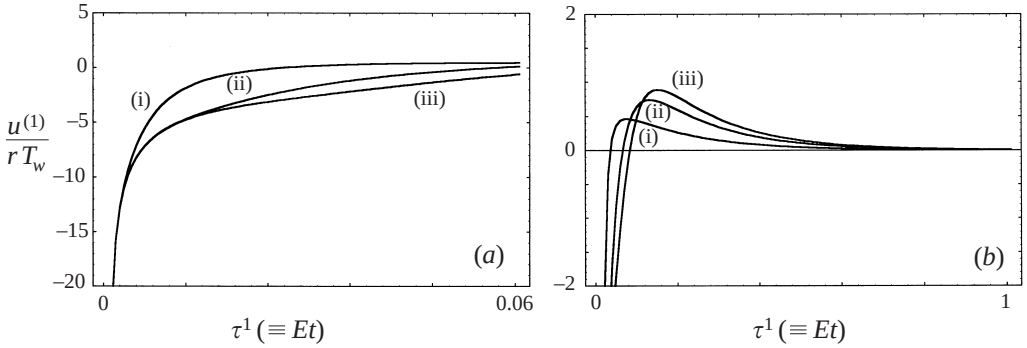

FIGURE 8. Evolution of radial velocity $u^{(1)}/r$ in the initial phase (a) and in the intermediate phase (b). $\sigma = 1.0$. The radial positions, r, are (i) 0.8; (ii) 0.5; (iii) 0.2.

process leads ultimately to the loss of angular momentum at the wall. Therefore, a fluid particle at a specific location moves radially inward initially and it moves radially outward later. By the time when this particle reaches its original position, due to the viscosity influenced loss of angular momentum during this excursion, the angular velocity of this fluid particle is lower than its original value, i.e. the angular velocity of the wall. This is represented in curves (ii) (at $\tau_1 = 0.3$) and (iii) (at $\tau_1 = 0.5$) of figure 7, which show negative values of $v^{(1)}$. (Obviously, at sufficiently large times, due to the diffusion of angular momentum from the wall, the entire flow field, together with the wall, is in rigid-body rotation. This implies $v^{(1)} \to 0$ everywhere at very large times.) The relative change in angular velocity over time is larger near the axis since the loss of angular momentum is pronounced in the near-axis region.

The time-histories of radial velocity are illustrated in figure 8. At small times (see figure 8(a)), since the thermal front is situated near the wall, the bulk of the flow field is inviscid, and $u^{(1)}/r$ is largely independent of r. For a fluid particle whose radial position is smaller than that of the thermal front, this fluid is pushed radially inward effectively by the expansion at very large radii. On the other hand, if the radial position of a particle is larger than that of the thermal front, volume expansions at smaller radii take place, which quickly offsets the radially inward motions. These are represented in figure 8(a), i.e. $u^{(1)}/r$ at a larger radius approaches zero at a faster rate than at a smaller radius.

The long-time behaviour of $u^{(1)}$ over the diffusion timescale is depicted in figure 8(b). As stated, in the early stage, $u^{(1)}$ is negative, i.e. directed radially inward, due to the expansion of the near-wall fluid. Consider a fluid particle at a specific radial location r_p. From $t = 0$ to the moment when the thermal front arrives at r_p, i.e. over the period when the thermal front is situated between $r = r_p$ and $r = 1$, the fluid particle undergoes thermo-acoustic compression, which generates the radially inward motion. When the thermal front has passed this location r_p radially inward, the fluid at $r < r_p$ expands, which contributes to the generation of radially outward velocity at r_p. The overall radial velocity at a specific location, therefore, crosses zero at an intermediate time. Afterward, the radially outward velocity outweighs the radially inward velocity, as shown in figure 8(b). At still larger times, the global flow field settles down to the final steady state, and $u^{(1)}$ tends to zero accordingly. The switchover of $u^{(1)}$ from the radially inward direction to the radially outward direction takes place earlier for a fluid particle located at a further radial position.

The time history of angular velocity, $v^{(1)}/r$, is displayed in figure 9 as solid lines. For reference, the temperature is shown as dashed lines. Figure 9(a) pertains to the

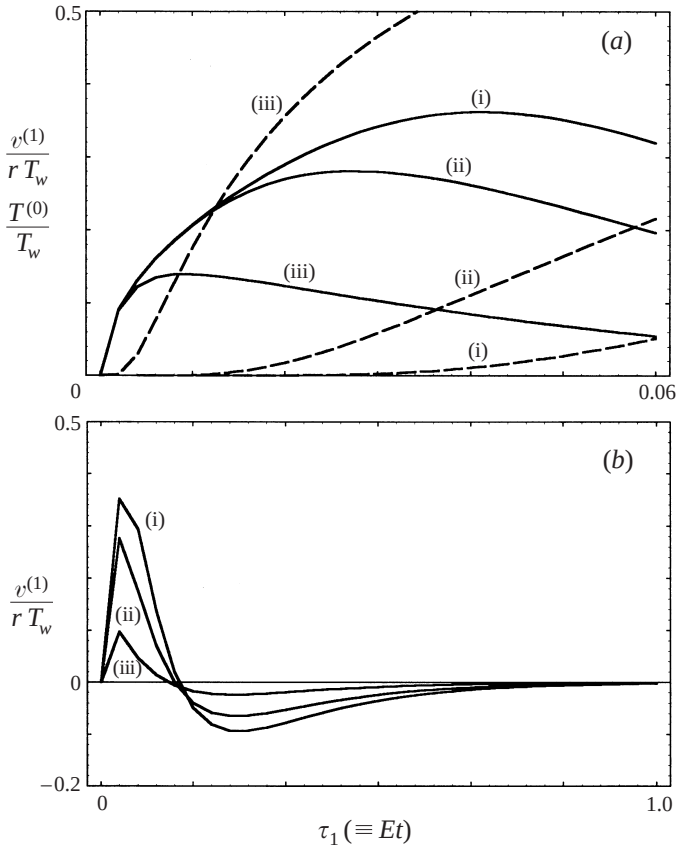

FIGURE 9. Evolution of angular velocity $v^{(1)}/r$ in the initial phase (a) and in the intermediate phase (b). $\sigma = 1.0$. In (a) ———, angular velocity and — — —, temperature. The radial positions, r, are: (i) 0.2; (ii) 0.5; (iii) 0.8.

early phase. This picture reinforces the assertions on the propagation of the thermal front and the selective expansion of fluid in the regions ahead of and behind the front. As ascertained, for a fluid particle at a specific location r_p, until the arrival of the thermal front, the radial velocities are radially inward. This gives rise to a rapid build-up of angular velocity (note the slope of $v^{(1)}$ curves in figure 9a). The major mechanism here is based on the conservation of angular momentum, which is in line with the isothermal–isentropic process. After the thermal front has passed this location, expansion takes place in the inner region ahead of the front, which contributes to the generation of radially outward motion at r_p. Consequently, a decrease of angular velocity results. It is again emphasized that this is a viscosity-influenced process in which conservation of angular momentum does not hold. The overall evolution of $v^{(1)}/r$ over the diffusion timescale is shown in figure 9(b). At small times, due to the presence of radially inward flow, the angular velocity increases based on the isothermal–isentropic process in which the angular momentum is conserved. At intermediate times, the viscously controlled diffusion of angular momentum takes place. In this phase, the angular velocity decreases accordingly, and the fluid particle experiences radially outward motion. By the time when the fluid particle returns to its original position, the angular velocity is negative, which reflects the afore-mentioned loss of angular momentum over the period. At still later times, the angular velocity

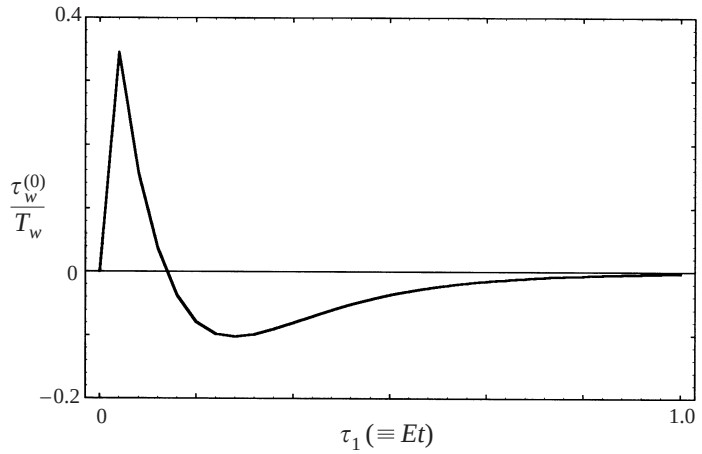

FIGURE 10. Evolution of wall shear stress $\tau_w^{(0)}$. $\sigma = 1.0$.

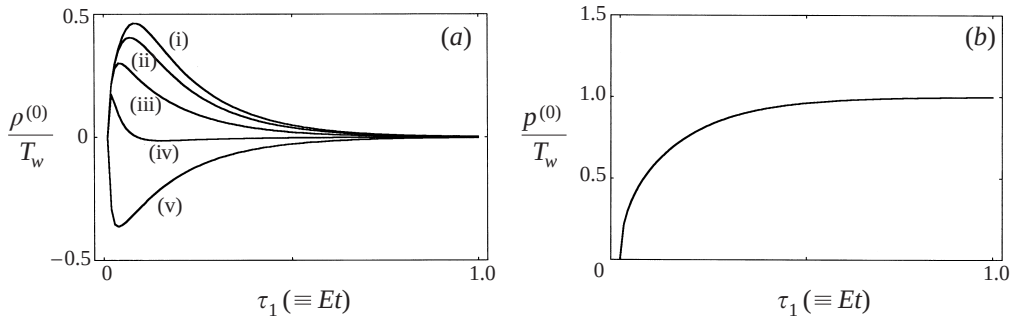

FIGURE 11. Evolution of density $\rho^{(0)}$ (*a*) and pressure $p^{(0)}$ (*b*). $\sigma = 1.0$. In (*a*), the radial positions, r, are (i) 0.1; (ii) 0.3; (iii) 0.5; (iv) 0.7; (v) 0.9.

at a location slowly regains angular momentum which is diffused from the wall. At a very long time, both the fluid and the wall are in solid-body rotation, and $v^{(1)}$ approaches zero. The above physical rationalization is revealing. In summary, at small times, the fluid rotates faster than the wall: the wall imparts a frictional drag to the fluid. At intermediate and large times, the angular velocity of the fluid is lower than that of the wall: the fluid imparts a frictional drag to the wall.

It is useful to define the wall shear stress τ_w from (41*a*)–(41*b*):

$$\tau_w = \frac{\tau_w^*}{E\rho_{00}^*(R_0)(\Omega R_0)^2} = -\frac{1}{M^2}\frac{\mathrm{d}v}{\mathrm{d}r},$$

in which superscript $*$ denotes dimensional quantities. It then follows that

$$\tau_w = \tau_w^{(0)} + O(M^2) = -\left(\frac{\mathrm{d}v^{(1)}}{\mathrm{d}r}\right)_{r=1.0} + O(M^2). \tag{51}$$

The evolution of τ_w is plotted in figure 10. As delineated in the above, at small times τ_w is positive, for which the wall produces frictional resistance for the fluid. At intermediate times, τ_w is negative, in which the wall rotates faster than the fluid. At still larger times, the fluid and the wall reach solid-body rotation, and τ_w vanishes. This behaviour is unique to a compressible fluid. For an incompressible fluid, no

change in τ_w is expected due to a sudden alteration of the wall temperature. The crux of the argument is that, for a compressible fluid, a step-change in wall temperature brings about both the transfer of angular momentum and the conventional heat transfer through the wall.

The overall evolution of density $\rho^{(0)}$ and pressure $p^{(0)}$ is portrayed in figures 11(*a*) and 11(*b*), respectively. At very small times, in the near-wall region, density decreases due to the expansion caused by the temperature increase. In the inner region, the fluid undergoes the thermo-acoustic compression, which leads to an increase in $\rho^{(0)}$. At intermediate times, the thermal front moves close to the axis, and the temperature in the inner region increases, which gives rise to an expansion. In summary, in the near-wall region, $\rho^{(0)}$ decreases in the early phase and $\rho^{(0)}$ increases at intermediate times. In the near-axis inner region, a qualitatively opposite process is discernible. At still larger times, as the final steady state is approached, $\rho^{(0)}$ tends to zero, and the density field regains the initial profile.

As is evident in (36), the lowest-order pressure field is spatially uniform, which is reflected in figure 11(*b*). The physical explanation is that, if a spatially non-uniform pressure field is present, a pressure wave, which propagates at the sonic velocity, is developed in order to smooth out this non-uniformity. Thus, the timescale for the removal of spatial-non-uniformity of the pressure field is given as $O(M)$, which is far shorter than the overall diffusion timescale $O(E^{-1})$. It is recalled that the present discussion is concerned with times of $O(E^{-1})$, which points to the existence of a spatially uniform pressure field. At very large times approaching the steady state, $p^{(0)} \to T_w$, $\rho^{(0)} \to 0$, which implies that the effect of the imposition of T_w at the wall ultimately appears in a global increase of pressure.

7. Conclusions

The transient adjustment process of a compressible fluid in a rapidly rotating pipe is studied. The motion is initiated by imposing a step-change in the wall temperature T_w.

Over times of $O(E^{-1/2})$, near the wall a thermal boundary layer of thickness $O(E^{1/4})$ exists, and a radial velocity of $O(E^{3/4})$ is developed. The disturbance propagates into the bulk of the interior in the form of thermo-acoustic compression. This interior motion is an inviscid isentropic process in which angular momentum is conserved. On this timescale, in the inviscid interior, $v, \rho, p \sim O(E^{1/4})$, $u \sim O(E^{3/4})$ and $T \sim O(E^{1/2})$.

Over diffusive times of $O(E^{-1})$, the mechanism is far more complex and intriguing. At times before the thermal front has reached the axis, the flow domain can be divided into two regions. One is the inviscid region ahead of the front, in which the afore-mentioned thermo-acoustic compression continues to prevail. The other is the viscous region behind the front, in which conservation of angular momentum no longer holds. After the thermal front has reached the axis, the entire flow field is viscously influenced. In the near-axis zone, the temperature increases rapidly toward the final steady state, which causes a volume expansion. Therefore, a radially outward flow is generated. In summary, at early times, the fluid rotates faster than the wall; but at intermediate times, the rotation rate of fluid is lower than that of the wall. At still larger times, both the fluid and the wall approach solid-body rotation.

REFERENCES

Bark, F. H. & Bark, T. H. 1976 On vertical boundary layers in a rapidly rotating gas. *J. Fluid Mech.* **78**, 815–825.

Bark, F. H., Meijer, P. S. & Cohen, H. I. 1979 Spin-up of a rapidly rotating gas. *Phys. Fluids.* **21**, 531–539.

Batchelor, G. K. 1967 *An Introduction to Fluid Dynamics.* Cambridge University Press.

Carslaw, H. S. & Jaeger, J. C. 1959 *Conduction of Heat in Solids.* Oxford University Press.

Frankel, L. E. 1959 A cylindrical sound pulse in a rotating gas. *J. Fluid Mech.* **11**, 637–649.

Gans, R. F. 1974 On the Poincaré problem for a compressible medium. *J. Fluid Mech.* **62**, 657–675.

Gans, R. F. 1975 On the stability of shear flow in a rotating gas. *J. Fluid Mech.* **68**, 403–412.

Greenspan, H. P. & Howard, L. N. 1963 On a time-dependent motion of a rotating fluid. *J. Fluid Mech.* **17**, 385–404.

Hultgren, L. S., Meijer, P. S. & Bark, F. H. 1981 On axisymmetric time-dependent source flows in a rapidly rotating gas. *J. Méc.* **20**, 135–157.

Hyun, J. M. & Park, J. S. 1989 Some aspects of compressible Rayleigh's problem in a rotating cylinder. *J. Phys. Soc. Japan* **58**, 159–166.

Hyun, J. M. & Park, J. S. 1992 Spin-up from rest of a compressible fluid in a rapidly rotating cylinder. *J. Fluid Mech.* **237**, 413–434.

Lalas, D. P. 1975 The 'Richardson' criterion for compressible swirling flows. *J. Fluid Mech.* **69**, 65–72.

Miles, J. W. 1981 Waves in a rapidly rotating gas. *J. Fluid Mech.* **107**, 487–497.

Morton, J. B. & Shaughnessy, E. J. 1972 Waves in a gas in solid-body rotation. *J. Fluid Mech.* **56**, 277–286.

Nakayama, W. & Usui, S. 1974 Flow in rotating cylinder of a compressible fluid. *J. Nuclear Sci. Tech.* **11**, 242–262.

Ozoe, H., Sato N. & Churchill, S. W. 1980 The effect of various parameters in thermo-acoustic convection. *Chem. Engng Commun.* **5**, 203–221.

Park, J. S. & Hyun, J. M. 1989. Transient adjustment of a gas contained in a rapidly-rotating infinite cyclinder. *J. Phys. Soc. Japan* **58**, 3949–3959.

Park, J. S. & Hyun, J. M. 1997 Transient Stewartson layers of a compressible fluid in a rapidly rotating cylinder. *Fluid Dyn. Res.* **19**, 303–325.

Park, J. S. & Hyun, J. M. 1998 Transient sidewall shear layers of compressible fluid in a rapidly rotating cylinder. *Fluid Dyn. Res.* **22**, 231–250.

Sakurai, T. & Matsuda, T. 1974 Gasdynamics of a centrifugal machine. *J. Fluid Mech.* **62**, 727–736.

Spradley, L. W. & Churchill, S. W. 1975 Pressure and buoyancy driven thermal convection in a rectangular enclosure. *J. Fluid Mech.* **70**, 705–720.

Torii, S. & Yang, W. J. 1994 A numerical analysis on flow and heat transfer in the entrance region of an axially rotating pipe. *ISROMAC-5* (*Hawaii, USA*) (ed. J. H. Kim & W. J. Yang), vol. **A**, pp. 593–605.